Exact step-coupling theory for mode-coupling behavior in geometrical variation photonic crystal waveguides

E. H. Khoo,[1,2] A. Q. Liu,[1,*] X. M. Zhang,[1] E. P. Li,[2] J. Li,[3] D. Pinjala,[3] and B. S. Luk'yanchuk[4]
[1]*School of Electrical and Electronic Engineering, Nanyang Technological University, Nanyang Avenue, Singapore 639798, Singapore*
[2]*Institute of High Performance Computing, 1 Fusionopolis Way, Connexis, Singapore 138632, Singapore*
[3]*Institute of Microelectronics, 11 Science Park Road, Singapore 117685, Singapore*
[4]*Data Storage Institute, DSI Building, 5 Engineering Drive 1, Singapore 117608, Singapore*
(Received 18 November 2008; revised manuscript received 27 May 2009; published 1 July 2009)

In this paper, an exact step-coupling theory is developed to describe the modes coupling behavior and lightwaves propagation for the power exchange between the waveguide modes in geometrical variation photonic crystal waveguide. The exact step-coupling theory provides a general description of the mode-coupling mechanism for light waveguide with geometrical variation with complete set of equations and solutions. The coupling equations of the exact step theory are derived and compared with the scattering matrix method, where simulation results show good agreement with an error of less than 2.2%. Subsequently, the coupling equations are applied to different case studies such as slab tapered waveguide and lossy "turn-on" waveguide. The transmission spectrum and field pattern distribution show that the lossy waveguide has a large radiation loss with an average transmission efficiency of less than 5%. The slab tapered waveguide can have more than 90% transmission efficiency with the convex curvature. The exact step-coupling theory can be applied to a vast range of geometrical variation photonic crystal based waveguides and it has quick and accurate convergence simulation results.

DOI: 10.1103/PhysRevB.80.035101 PACS number(s): 42.70.Qs, 42.79.Gn

I. INTRODUCTION

In the last two decades, a new field of research called the photonic crystal (PC)[1,2] has emerged. By introducing a row of defect structures into the bulk PC, the translational symmetry is broken and defect mode(s) are introduced into the photonic band gap (PBG). The lightwave is only allowed to propagate in the row defect sites. These photonic crystal based waveguides (PCWGs) are reported[3,4] that can guide light around sharp corners with very low transmission loss.[5] By incorporating with other defect structures, a series of PCWG based devices are innovated such as directional coupler, optical filter, wide-angle splitters, and nonlinear amplification.[6–10]

However, many challenges arise in the aspects of design, fabrication, characterization, and measurement for the narrow single mode PCWG. Apart from these, it is also important for high coupling efficiency between the light source and PCWG. The different waveguide shape and size cause large impedance mismatch between the light source and PCWG, which resulted in a large amount of lightwaves reflection and scattering.

In order to achieve high coupling efficiency between the light source and narrow PCWG, many coupling techniques[11–17] have been developed to improve the coupling transmission efficiency. Among these coupling techniques, the photonic crystal tapered waveguides (PCTWs)[18–23] are often used. The guiding mechanism in PCTW is based on the presence of guided modes in photonic band gap, which is a different concept from conventional dielectric taper.

The advantages of PCTW are as follows: first, shorter taper length can be used to couple lightwaves[18] from source to PCWG. Second, impedance mismatch is reduced between PCTW and PCWG due to identical structural definition. Third, the curvature of the taper[21] can be manipulated to obtain higher coupling efficiency. Fourth, PCTW may also support a larger range of frequencies compared to the conventional dielectric tapered waveguide.[24]

For high effective coupling of the PCTW, two conditions to be satisfied are the following: first, at least one transmitted mode must be contained present in every part of the tapering section so as to ensure transmission through the tapering section. Second, the propagating modes must lie in the photonic band gap for every intermediate section of the PCTW so that the propagating modes are true guided modes and do not leak to the periodic surrounding.

To investigate the coupling behavior of different modes along the PCTW, semianalytical methods are formulated to explain the intercoupling mechanism and characteristics. Various semianalytical methods are available to analyze the mode-coupling and propagation behavior in tapered waveguides. One of the common semianalytical methods is the coupled mode theory,[25,26] which expands the electromagnetic field components into the eigenmodes of a waveguide and solve for the coupling amplitudes the geometrical variation waveguide. Together with perturbation theory, the coupled mode theory convergences very fast for gradual geometrical variation waveguide with gradual slope.[25] However, limitations occur for taper with steep slope because higher order corrections are required to achieve convergence to exact solutions. The other analytical methods such as the beam propagation methods[27] and the multipole method[28,29] also have been developed. The beam propagation method is easy to implement and is an efficient modeling tool for lightwave propagation calculation. However, its limited ability to accurately predict the backward propagation lightwaves and complicated interference of phase variation make it difficult for application in geometrical variation waveguide. For high-

index contrast waveguide, the multipole method[17,18] can be applied to analyze the eigenmodes with high numerical accuracy but it does not allow perturbative formulation. Hence, it is difficult to use the multipole method to explain the intermodal coupling behavior in the PCTW.

Step-theory method[30,31] is another popular theory for the analysis of waveguide with geometrical variation. This method divides the taper structure into piecewise strip called steps. Field components between steps are matched by imposing boundary conditions and then solved rigorously. The advantages of the step-theory are as follows: first, it studies the coupling mechanism between different propagating modes. Second, it is very simple to use for tapered waveguide. Third, it can calculate the transmission and reflection for different taper structures with high convergence rate and accuracy. The main drawback for the step-theory method is that when the taper length increases, the number of steps also increases. As a result, a longer computation time is required. Nevertheless, it is still useful for investigating the mode coupling and interaction in geometrical variation waveguide.

A modified step theory[31] was developed by incorporating Bloch theorem into the original step theory. In the course of derivation, several assumptions and approximations are made. These assumptions and approximations limit the application of the modified step theory to long length taper or slow taper. In this paper, a set of generalized coupling equations incorporating the step theory is derived and the intermodal coupling behavior for different waveguides will be investigated.

In the modified step theory, the intermodal coupling between the reflected modes is considered negligible for tapers structures with gradual slope, where the change in propagating wave vector $\Delta\beta$ is very slow. However, this is not valid for short length tapers, as well as taper structures with fast changing slope along the tapering direction because $\Delta\beta$ is relatively large. There is substantial amount of back reflected power in the tapered waveguide.

The second assumption states that the coupling between radiation modes and the guided modes in the tapered waveguide is negligible operating frequencies within the PBG. However, the guided modes operating near the edge of the PBG are subjected to possible mode coupling with the radiation mode in the bulk continuum.[31,32] Therefore, the modified step theory fails to provide an accurate modeling of the transmitted power for the PCTW near the edge of the PBG.

In the third assumption, power loss coupling between the two guided modes is neglected because the reflection loss is assumed to be the main loss component.[33] However, for longer taper, the reflection loss is reduced significantly due to slower change in the propagating wave vector, β. In this case, the intermodal coupling loss between the two guided modes dominates. The intermodal coupling occurs between one guided mode and another guided mode or radiation mode near the edge of the PBG. Therefore, power loss known as intermodal loss is observed.

In this paper, the objective is to rigorously derive a set of general coupling equations to describe the intermodal coupling behavior and characteristics of lightwaves in periodic geometrical variation PC structures. The structure of the paper is organized as follows: first, the solutions for the field in the waveguide are expanded in local normal modes and the step-theory principle is derived to obtain generalized coupling equations. Subsequently, the convergence of the coupling equations will be discussed. This is followed by a case study of the exact coupling equations of the step theory to photonic crystal slabs waveguide and lossy PCWG. The simulation results obtained using the exact step-coupling theory will be discussed.

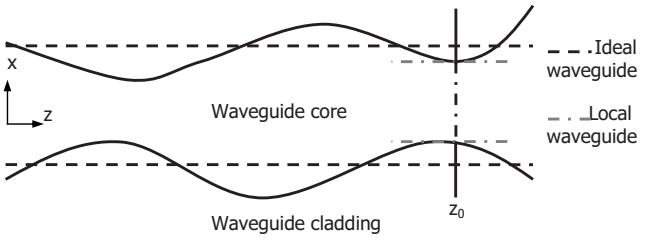

FIG. 1. Definition of ideal waveguide and local waveguide.

II. EXACT STEP-COUPLING THEORY

Before deriving the coupling equations for the exact step-coupling theory, it is essential to discuss the description of the electromagnetic fields in geometrical variation waveguide.[34–38] Using the normal modes, it requires the selection of the type of reference waveguide structure. There are two ways of setting the waveguide reference for the field description as shown in Fig. 1. The solid line shows the geometrical variation dielectric waveguide with varying core width. The normal field component of the varying width waveguide can be expanded in term of modes of the ideal waveguide shown as the dash line. This representation is called ideal waveguide normal mode representation. One characteristic of the representation is that the coefficients of the electromagnetic fields are function of z but the field components are constant.

There is an alternate way of describing the field components by expanding the fields in terms of modes belonging to a fictitious waveguide, which coincides locally at all the points of the waveguide. This means considering the fields for all points along the geometrical variation waveguide, as represented by the dash-dotted line in Fig. 1. At this point, the fields are expressed in terms of a hypothetical waveguide formed by the two dash-dotted lines. The normal modes of the hypothetical waveguide vary in width as a function of z.

Both types of field expansions have their own advantages for solving different types of waveguide variations. The field expansion in term of modes of an ideal waveguide is more preferred for waveguides with perfect geometries but refractive index variations. The coupling coefficients of ideal mode expansion are simple and can be computed easily. On the other hand, the coupling coefficients of electromagnetic field for local mode expansion are more complicated than the ideal mode waveguide because it considers the waveguide variation locally. The local mode expansion is more useful for a waveguide with geometrical variation than the ideal mode expansion. It is because a better description and analysis of the intermodal coupling behavior in geometrical varia-

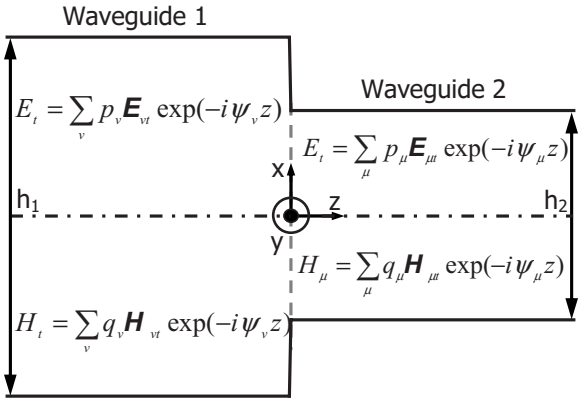

FIG. 2. Schematic diagram of the electromagnetic field components in two waveguides with different widths.

tion waveguide can be presented. Besides, local normal modes expansion has an additional advantage for PCTW as it is easy and simple to apply.

In this paper, the mode coupling in geometrical variation waveguide, specifically tapered waveguide, is seen as the propagation between waveguides of different widths. Figure 2 shows the schematic representation of the field components at the interface of two different waveguide widths. The boundary condition state of the electromagnetic field must be continuous across the interface. This is exceptional for the case of an ideal perfect conductor or superconductor medium on either side of the interface.[39]

For derivation of the coupling equation for the exact step-coupling theory, only the transverse components of the fields are required. Expanding the electromagnetic fields in series to account for the guided mode, the fields are expressed as

$$E_t(x,y,z) = \sum_\nu p_\nu(z)\mathbf{E}_{\nu t}(x,y)\exp(-i\psi_\nu z), \tag{1}$$

$$H_t(x,y,z) = \sum_\nu q_\nu(z)\mathbf{H}_{\nu t}(x,y)\exp(-i\psi_\nu z), \tag{2}$$

where ψ_ν is the propagation constant of the guide mode ν. The series expansion of the transverse mode field vector in Eqs. (1) and (2) applies to all modal polarizations, either TM or TE modes. The summation covers the entire guided modes of the waveguide as well as the integral over the entire bulk continuum range of radiation modes. From Eqs. (1) and (2), the amplitude coefficients, p_ν, and q_ν, are used to account for the z component of the electric field and magnetic field, respectively. The direction dependences of the electric and magnetic field p_ν and q_ν amplitude coefficients are omitted for simplicity. After applying the series field expansion into the curl Maxwell equations, the following expressions are obtained as

$$\nabla \times \left[\sum_\nu q_\nu \mathbf{H}_{\nu t}\exp(-i\psi_\nu z)\right] = -i\omega\varepsilon_0 \sum_\nu p_\nu \mathbf{E}_{\nu t}\exp(-i\psi_\nu z), \tag{3a}$$

$$\nabla \times \left[\sum_\nu p_\nu \mathbf{E}_{\nu t}\exp(-i\psi_\nu z)\right] = i\omega\mu_0 \sum_\nu q_\nu \mathbf{H}_{\nu t}\exp(-i\psi_\nu z). \tag{3b}$$

By expanding the operator ∇ into the form $\nabla = \nabla_t + e_z(\partial/\partial z)$, the following expressions are obtained:

$$\sum_\nu \left\{\left(\frac{1}{i\omega\mu}\right)\nabla_t \times [\nabla_t \times p_\nu \mathbf{E}_{\nu t}\exp(-i\psi_\nu z)] + e_z \times \frac{\partial[q_\nu \mathbf{H}_{\nu t}\exp(-i\psi_\nu z)]}{\partial z}\right\} = \sum_\nu -i\omega\varepsilon_0 p_\nu \mathbf{E}_{\nu t}\exp(-i\psi_\nu z), \tag{4a}$$

$$\sum_\nu \left\{-\left(\frac{1}{i\omega\varepsilon}\right)\nabla_t \times [\nabla_t \times q_\nu \mathbf{H}_{\nu t}\exp(-i\psi_\nu z)] + e_z \times \frac{\partial[p_\nu \mathbf{E}_{\nu t}\exp(-i\psi_\nu z)]}{\partial z}\right\} = \sum_\nu i\omega\mu_0 q_\nu \mathbf{H}_{\nu t}\exp(-i\psi_\nu z). \tag{4b}$$

The symbols ∇_t and e_z are the transverse and longitudinal components of ∇, respectively. From this point, the exponential components are omitted so as to simplify the notation for a clearer derivation. However, it is understood that this exponential component is added to the field expression. Because the expansion of the electromagnetic field is based on the local normal modes, the local field modes $\boldsymbol{E}$ and $\boldsymbol{H}$ are functions of z, contrary to the ideal mode expansion. By expanding and solving for the variable in the derivatives, Eq. (4) can be simplified as

$$\sum_\nu \left\{\left[ip_\nu\psi_\nu + \frac{\partial q_\nu}{\partial z}\right](e_z \times \mathbf{H}_{\nu t}) + (q_\nu)\left(e_z \times \frac{\partial \mathbf{H}_{\nu t}}{\partial z}\right)\right\} = 0, \tag{5a}$$

$$\sum_\nu \left\{\left[iq_\nu\psi_\nu + \frac{\partial p_{\nu t}}{\partial z}\right](e_z \times \mathbf{E}_{\nu t}) + (q_\nu)\left(e_z \times \frac{\partial \mathbf{E}_{\nu t}}{\partial z}\right)\right\} = 0. \tag{5b}$$

Equations (5a) and (5b) show the field expansion of the generalized Maxwell equation with the amplitude coefficients for mode ν. In order to obtain the coupling equation relating the waveguide modes of two different cross-sectional widths, orthogonal relation is applied. The expression for this relation is given by[35]

$$\int\int e_z \cdot (\mathbf{E}_{\nu t} \times \mathbf{H}^*_{\mu t})dxdy = 2\delta_{\nu\mu}P\frac{\psi^*_\mu}{|\psi_\mu|}, \tag{6}$$

where the subscripts μ and ν refer to the modes number at different cross-sectional waveguide widths. The double inte-

gral implies that the transverse electromagnetic field spans over the x and y transverse directions. The symbol $\delta_{\nu\mu}$ indicates the Kronecker's delta expression for discrete guided modes in the photonic band gap. For coupling between guided modes and the bulk continuum of the radiation modes outside the photonic band gap, it is the Dirac delta function. The ratio $\beta_\mu^*/|\beta_\mu|$ is used to indicate whether the mode coupling involves the radiation modes. When pure guided mode in the photonic band gap is considered, the ratio indicates +1 because the β values are real positive quantities. When the coupling involves the radiation mode that has imaginary β values, the ratio is complex and therefore the coupling equations are complex as well. P is the power factor of the propagating lightwaves.

To apply the orthogonal relationship, the scalar product of Eq. (5a) is taken with the complex conjugate of the mode electric field, $\mathbf{E}_\mu^*$. After applying the triple product vector identities and taking the integral over the transverse axis, the Maxwell equation is finally simplified as

$$\sum_\nu \left[ip_\nu\psi_\nu + \frac{\partial q_\nu}{\partial z} \right] \int\int e_z \cdot (\mathbf{H}_\nu \times \mathbf{E}_\mu^*) dxdy = \sum_\nu (q_\nu) \int\int -e_z \cdot \left(\frac{\partial \mathbf{H}_\nu}{\partial z} \times \mathbf{E}_\mu^* \right) dxdy. \tag{7}$$

It is not necessary to include the subscript t in Eq. (7) because the transverse field components are considered and the longitudinal components do not contribute to the z components of the cross product. Based on the orthogonal relationship in Eq. (6), Eq. (7) is simplified as

$$i\psi_\mu p_\mu + \frac{\partial q_\mu}{\partial z} = \sum_\nu R_{\nu\mu} q_\nu, \tag{8}$$

where the coupling coefficient $R_{\nu\mu}$ is given as

$$R_{\nu\mu} = \frac{-|\psi_\mu|}{2P\psi_\mu} \int\int e_z \cdot \left(\mathbf{E}_\mu^* \times \frac{\partial \mathbf{H}_\nu}{\partial z} \right) dxdy. \tag{9}$$

The coupling coefficient $R_{\nu\mu}$ means the coupling of the mode label ν to the mode μ. Using the same procedure for Eq. (5b) by taking the scalar product with $\mathbf{H}_\mu^*$, it is expressed as

$$i\psi_\mu q_\mu + \frac{\partial p_\mu}{\partial z} = \sum_\nu S_{\nu\mu} p_\nu, \tag{10}$$

where the coupling coefficient $S_{\nu\mu}$ is given as

$$S_{\nu\mu} = \frac{-|\psi_\mu|}{2P\psi_\mu^*} \int\int e_z \cdot \left(\frac{\partial \mathbf{E}_\nu}{\partial z} \times \mathbf{H}_\mu^* \right) dxdy. \tag{11}$$

The series expansion of the electromagnetic field in the Maxwell equation gave two sets of coupling equations [Eqs. (8) and (10)] that contain the field amplitude coefficients, p and q. When $S_{\nu\mu}$ and $R_{\nu\mu}$ are zero (absence of coupling), the amplitude coefficients p and q can be solved. After transforming the first-order differential equations into the second order through internal substitution and solving, the field amplitude coefficients p_μ and q_μ are obtained as

$$p_\mu = p_\mu^{(+)} = c_\mu^{(+)} \exp(-i\psi_\mu z) \tag{12a}$$

$$p_\mu = p_\mu^{(-)} = c_\mu^{(-)} \exp(i\psi_\mu z) \tag{12b}$$

$$q_\mu = q_\mu^{(+)} = c_\mu^{(+)} \exp(-i\psi_\mu z) = p_\mu^{(+)} \tag{13a}$$

$$q_\mu = q_\mu^{(-)} = -c_\mu^{(-)} \exp(i\psi_\mu z) = -p_\mu^{(-)} \tag{13b}$$

The p and q coefficients are slow traveling wave components of electromagnetic field. When substituting Eqs. (12) and (13) into Eqs. (1) and (2), respectively, the exponential term is not included. There exist two possible solutions for each of the amplitude coefficients, p_μ and q_μ. The plus superscript (+) and the minus superscript (–) indicate a traveling wave in the positive or negative z direction. From Eqs. (12a) and (13a), it can be seen that the first set of solutions for the amplitude coefficients q_μ and p_μ are identical. However, the second set of solutions is differentiated by the presence of a negative sign. It is to provide an explanation for the use of a different amplitude coefficient for the magnetic-field expansion. It is because the sign for backward traveling transverse magnetic field is reversed. On the other hand, the single amplitude coefficient is used to describe the transverse (z) field components for the electric field in both the forward and backward directions and another coefficient for the magnetic field. This is justified by the fact that each mode must behave as an entity.[33] According to the field theory, all field components of each mode must change at the same rate since otherwise the mode will lose its identity. According to Eqs. (12) and (13), the mode field can be defined as

$$\beta_\mu^{(+)} = \beta_\mu, \tag{14a}$$

$$\beta_\mu^{(-)} = -\beta_\mu, \tag{14b}$$

$$\mathbf{E}_\mu^{(+)} = \mathbf{E}_\mu^{(-)} = \mathbf{E}_\mu, \tag{14c}$$

$$\mathbf{H}_\mu^{(-)} = -\mathbf{H}_\mu^{(+)} = -\mathbf{H}_\mu. \tag{14d}$$

From the solutions of Eqs. (12) and (13), it can be seen that the forward and backward propagating waves can be separated by the transformation equation expressed as

$$p_\mu = p_\mu^{(+)} + p_\mu^{(-)}, \tag{15a}$$

$$q_\mu = p_\mu^{(+)} - p_\mu^{(-)}. \tag{15b}$$

Substituting Eq. (15) into Eqs. (8) and (10), the coupling equations in terms of the forward and backward traveling waves can be expressed as

$$\frac{\partial p_\mu^{(+)}}{\partial z} + i\psi_\mu p_\mu^{(+)} - \left[\frac{\partial p_\mu^{(-)}}{\partial z} - \psi_\mu p_\mu^{(-)}\right] = \sum_\nu R_{\nu\mu}(p_\nu^{(+)} - p_\nu^{(-)}), \tag{16a}$$

$$\frac{\partial p_\mu^{(+)}}{\partial z} + i\psi_\mu p_\mu^{(+)} + \left[\frac{\partial p_\mu^{(-)}}{\partial z} - i\psi_\mu p_\mu^{(-)}\right] = \sum_\nu S_{\nu\mu}(p_\nu^{(+)} + p_\nu^{(-)}). \tag{16b}$$

Adding and subtracting Eqs. (16a) and (16b) together, the coupling equations for the forward and backward waves can be obtained as

$$\frac{\partial p_\mu^{(+)}}{\partial z} = -i\psi_\mu p_\mu^{(+)} + \sum_\nu \vartheta_{\nu\mu}^{(+,+)} p_\nu^{(+)} + \vartheta_{\nu\mu}^{(+,-)} p_\nu^{(-)}, \tag{17a}$$

$$\frac{\partial p_\mu^{(-)}}{\partial z} = i\psi_\mu p_\mu^{(-)} + \sum_\nu \vartheta_{\nu\mu}^{(-,+)} p_\nu^{(-)} + \vartheta_{\nu\mu}^{(-,-)} p_\nu^{(-)}, \tag{17b}$$

where ϑ represents the overall coupling coefficient between the forward and backward waves. It relates to the coupling coefficients $R_{\nu\mu}$ and $S_{\nu\mu}$ expressed as

$$\begin{aligned}\vartheta_{\nu\mu}^{(\alpha,\gamma)} &= \alpha\gamma R_{\nu\mu} + S_{\nu\mu} \\ &= \left[\frac{-|\psi_\mu|}{2P\psi_\mu^{(\alpha)}}\int\int e_z \cdot \left(\mathbf{E}_\mu^{(\alpha)*} \times \frac{\partial \mathbf{H}_\nu^{(\gamma)}}{\partial z}\right) dxdy\right] \\ &\quad \times \frac{-|\psi_\mu|}{2P\psi_\mu^{(\alpha)*}}\int\int e_z \cdot \left(\frac{\partial \mathbf{E}_\nu^{(\gamma)}}{\partial z} \times \mathbf{H}_\mu^{(\alpha)*}\right) dxdy,\end{aligned} \tag{18}$$

where α and γ indicate the directions of the lightwaves in waveguide. When it is expressed as a factor, it has a value of +1 or −1. When it is a positive or negative sign, it indicates the direction of the coupling coefficient that is being evaluated. From Eqs. (17a) and (17b), it is observed that the amplitude coefficients of $p_\mu^{(+)}$ and $p_\mu^{(-)}$ are actually rapidly varying functions of z in the absence of coupling. Hence, the parameters $c_\mu^{(+)}$ and $c_\mu^{(-)}$ are constant in the absence of coupling. However, when there is coupling between modes, $c_\mu^{(+)}$ and $c_\mu^{(-)}$, their derivatives are present. Substituting $p_\mu^{(+)}$ and $p_\mu^{(-)}$ into Eq. (17), the coupling equation is obtained as

$$\begin{aligned}\frac{\partial c_\mu^{(+)}}{\partial z} &= \sum_\nu \vartheta_{\nu\mu}^{(+,+)} c_\nu^{(+)} \exp[iz(\psi_\mu - \psi_\nu)] \\ &\quad + \vartheta_{\nu\mu}^{(+,-)} c_\nu^{(-)} \exp[iz(\psi_\mu + \psi_\nu)],\end{aligned} \tag{19a}$$

$$\begin{aligned}\frac{\partial c_\mu^{(-)}}{\partial z} &= \sum_\nu \vartheta_{\nu\mu}^{(-,+)} c_\nu^{(+)} \exp[iz(\psi_\mu + \psi_\nu)] \\ &\quad - \vartheta_{\nu\mu}^{(-,-)} c_\nu^{(-)} \exp[iz(\psi_\nu - \psi_\mu)].\end{aligned} \tag{19b}$$

Equation (19) presents the general case of the coupling equations. It is important to highlight in Eq. (19) the absence of integral at the exponential phase coefficient. In contrast, other coupling equations[20] derived by different methods have an integral due to continuous evaluation of the phase coefficient. This absence of integral at exponential coefficient is due to the discrete nature of the exact step-coupling theory. It can provide a deeper understanding of the coupling mechanism for the geometrical variation waveguide section and can be easily simulated.

A. Simplification of the overall coupling coefficient ϑ

Based on the exact step-coupling equations shown in Eq. (19), the various intermodal coupling mechanisms of PCTW can be described and modeled. However, the forms for the overall coupling coefficient in Eq. (19) look rather awkward due to the presence of the curl terms. This makes it rather inconvenient to evaluate the exact step-coupling equation shown in Eq. (19). Therefore, a transformation is proposed to simplify the overall coupling coefficient $\vartheta_{\nu\mu}$. At the beginning of the derivation, the transverse part of the electromagnetic field components is used to directly derive the coupling equations. However, the longitudinal component is substituted into Eqs. (1) and (2) and then simplified with the local mode solutions that can be expressed as

$$\nabla_t \times \mathbf{H}_\mu - i\psi_\mu(e_z \times \mathbf{H}_\mu) = -i\omega\varepsilon\mathbf{E}_\mu, \tag{20a}$$

$$\nabla_t \times \mathbf{E}_\mu - i\psi_\mu(e_z \times \mathbf{E}_\mu) = i\omega\mu\mathbf{H}_\mu. \tag{20b}$$

It is noted that the local mode field does not satisfy these field equations. This can be overcome when the summation of all the modes is included in the final coupling equation as shown in Eq. (19). Therefore, the electromagnetic fields in Eq. (20) in complex conjugate form with the α superscript are expressed as

$$\nabla_t \times \mathbf{H}_\mu^{*(\alpha)} - i\psi_\mu^{*(\alpha)}(e_z \times \mathbf{H}_\mu^{*(\alpha)}) = -i\omega\varepsilon\mathbf{E}_\mu^{*(\alpha)}, \tag{21a}$$

$$\nabla_t \times \mathbf{E}_\mu^{*(\alpha)} - i\psi_\mu^{*(\alpha)}(e_z \times \mathbf{E}_\mu^{*(\alpha)}) = i\omega\mu\mathbf{H}_\mu^{*(\alpha)}. \tag{21b}$$

To obtain an expression that looks like the right side of Eq. (18), first take the scalar product of Eq. (21a) with the derivative $-d\mathbf{E}_\nu^{(\gamma)}/dz$ and Eq. (21b) with $d\mathbf{H}_\nu^{(\gamma)}/dz$. Then apply the triple product vector identities and adding up, it is obtained as

$$\begin{aligned}&-i\psi_\mu^{*(\alpha)}\left\{e_z \cdot \left[\left(\frac{\partial \mathbf{E}_\nu^{(\gamma)}}{\partial z} \times \mathbf{H}_\mu^{*(\alpha)}\right) + \left(\partial\frac{\mathbf{H}_\nu^{(\gamma)}}{\partial z} \times \mathbf{E}_\mu^{*(\alpha)}\right)\right]\right\} \\ &= i\omega\varepsilon\frac{\partial \mathbf{E}_\nu^{(\gamma)}}{\partial z} \cdot \mathbf{E}_\mu^{*(\alpha)} + i\omega\mu\frac{\partial \mathbf{H}_\nu^{(\gamma)}}{\partial z} \cdot \mathbf{H}_\mu^{*(\alpha)} \\ &\quad + \nabla_t \cdot \left[\left(\mathbf{H}_\mu^{*(\alpha)} \times \frac{\partial \mathbf{E}_\nu^{(\gamma)}}{\partial z}\right) + \left(\frac{\partial \mathbf{H}_\nu^{(\gamma)}}{\partial z} \times \mathbf{E}_\mu^{*(\alpha)}\right)\right].\end{aligned} \tag{22}$$

The left side of Eq. (22) has the same form as the right side of Eq. (18). On the right of Eq. (22), the operator ∇_t only operates on the electromagnetic field but not on its derivative. It is desirable to let ∇_t operate on all the field terms so as to apply the divergence properties to eliminate it. Therefore, when Eq. (20) is set to be dependent on the γ parameter for the mode label ν and then the derivative is taken with respect to z, it is obtained as

$$\nabla_t \times \frac{\partial \mathbf{H}_\nu^{(\gamma)}}{\partial z} - i\psi_\nu^{(\gamma)}\left(e_z \times \frac{\partial \mathbf{H}_\nu^{(\gamma)}}{\partial z}\right) - i(e_z \times \mathbf{H}_\nu^{(\gamma)})\frac{\partial \psi_\nu^{(\gamma)}}{\partial z} = -i\omega\varepsilon\frac{\partial \mathbf{E}_\nu^{(\gamma)}}{\partial z} - i\omega\mathbf{E}_\nu^{(\gamma)}\frac{\partial \varepsilon}{\partial z}, \tag{23a}$$

$$\nabla_t \times \frac{\partial \mathbf{E}_\nu^{(\gamma)}}{\partial z} - i\psi_\nu^{(\gamma)}\left(e_z \times \frac{\partial \mathbf{E}_\nu^{(\gamma)}}{\partial z}\right) - i(e_z \times \mathbf{E}_\nu^{(\gamma)})\frac{\partial \psi_\nu^{(\gamma)}}{\partial z} = i\omega\mu\frac{\partial \mathbf{H}_\nu^{(\gamma)}}{\partial z}. \tag{23b}$$

From Eq. (23), it can be seen that the phase coefficient ψ_ν is a function of z. At the moment, this term is left intact, but in the later part, it will vanish. Equation (23) also shows that the dielectric constant ε is also a function of z. This term is important and accounts for the dielectric discontinuities in the periodic PC structures. Again after taking the scalar product of Eq. (23a) with $\mathbf{E}_\mu^{(\alpha)^*}$ and Eq. (23b) with $-\mathbf{H}_\mu^{(\alpha)^*}$ and adding the resultant equations, the sum is obtained as

$$i\psi_\nu^{(\gamma)}\left\{e_z \cdot \left[\left(\frac{\partial \mathbf{E}_\nu^{(\gamma)}}{\partial z} \times \mathbf{H}_\mu^{*(\alpha)}\right) + \left(\mathbf{E}_\mu^{*(\alpha)} \times \frac{\partial \mathbf{H}_\nu^{(\gamma)}}{\partial z}\right)\right]\right\} = -i\omega\varepsilon\frac{\partial \mathbf{E}_\nu^{(\gamma)}}{\partial z} \cdot \mathbf{E}_\mu^{*(\alpha)} - i\omega\mu\frac{\partial \mathbf{H}_\nu^{(\gamma)}}{\partial z} \cdot \mathbf{H}_\mu^{*(\alpha)} - i\omega\mathbf{E}_\nu^{(\gamma)} \cdot \mathbf{E}_\mu^{*(\alpha)}\frac{\partial \varepsilon}{\partial z}. \tag{24}$$

The left side of Eq. (24) is the same form as Eq. (18) for the overall coupling coefficient. Adding Eqs. (22) and (24) and taking double integral, the resultant expression is obtained as

$$\int\int i(\psi_\nu^{(\gamma)} - \psi_\mu^{*(\alpha)})e_z \cdot \left[\left(\frac{\partial \mathbf{E}_\nu^{(\gamma)}}{\partial z} \times \mathbf{H}_\mu^{*(\alpha)}\right) + \left(\mathbf{E}_\mu^{*(\alpha)} \times \frac{\partial \mathbf{H}_\nu^{(\gamma)}}{\partial z}\right)\right]dxdy = \int\int \nabla_t \cdot \left[\left(\mathbf{H}_\mu^{*(\alpha)} \times \frac{\partial \mathbf{E}_\nu^{(\gamma)}}{\partial z}\right) + \left(\frac{\partial \mathbf{H}_\nu^{(\gamma)}}{\partial z} \times \mathbf{E}_\mu^{*(\alpha)}\right)\right]dxdy + \int\int i\frac{\partial \psi_\nu^{(\gamma)}}{\partial z}e_z \cdot [(\mathbf{H}_\mu^{*(\alpha)} \times \mathbf{E}_\nu^{(\gamma)}) + (\mathbf{H}_\nu^{(\gamma)} \times \mathbf{E}_\mu^{*(\alpha)})]dxdy - \int\int i\omega\mathbf{E}_\nu^{(\gamma)} \cdot \mathbf{E}_\mu^{*(\alpha)}\frac{\partial \varepsilon}{\partial z}dxdy. \tag{25}$$

The left side of Eq. (25) is identical to the overall coupling coefficient ϑ and is multiplied by a factor of the phase difference between the modes ν and μ. On the right side of Eq. (25), there are three terms, two of which would disappear by applying the orthogonal condition and divergence theorem. The first term is given as

$$\int\int \nabla_t \cdot \left[\left(\mathbf{H}_\mu^{*(\alpha)} \times \frac{\partial \mathbf{E}_\nu^{(\gamma)}}{\partial z}\right) + \left(\frac{\partial \mathbf{H}_\nu^{(\gamma)}}{\partial z} \times \mathbf{E}_\mu^{*(\alpha)}\right)\right]dxdy. \tag{26a}$$

These divergence terms in Eqs. (22) and (24) complement each other. When it is taken double integral over the xy plane, the divergence can be converted from the surface integral to the line integral around the waveguide, which is called the Strokes' theorem. The line integral vanishes for all guided modes, for all radiation modes and guided-radiation modes for $\nu \neq \mu$. Hence, the first term does not contribute to the coupling coefficient. The second term is given as

$$\int\int i\frac{\partial \psi_\nu^{(\gamma)}}{\partial z}e_z \cdot [(\mathbf{H}_\mu^{*(\alpha)} \times \mathbf{E}_\nu^{(\gamma)}) + (\mathbf{H}_\nu^{(\gamma)} \times \mathbf{E}_\mu^{*(\alpha)})]dxdy. \tag{26b}$$

It is obvious that the second term does not contribute to the coupling coefficient because it vanishes by applying the orthogonal relationship in Eq. (6) for the guided modes as well as the radiation modes. If $\nu \neq \mu$, the third term is given as

$$\int\int i\omega\mathbf{E}_\nu^{(\gamma)} \cdot \mathbf{E}_\mu^{*(\alpha)}\frac{\partial \varepsilon}{\partial z}dxdy. \tag{26c}$$

It defines the coupling coefficient in the scalar product form. As mentioned earlier in the paper, the presence of curl terms can be removed from the overall coupling coefficient in Eq. (18) and simplified by the scalar product of the mode field. The derivative $\partial\varepsilon/\partial z$ accounts for the periodic dielectric discontinuities in the PC lattice. The absence of the derivative for the magnetic permeability, $\partial\mu/\partial z$, is because the waveguiding material is assumed to be nonmagnetic. Therefore, the overall coupling coefficient is re-expressed as

$$\vartheta_{\nu\mu}^{(\alpha,\gamma)} = \frac{\omega\alpha|\psi_\mu^{*(\alpha)}|}{2P\psi_\mu^{*(\alpha)}(\psi_\mu^{*(\alpha)} - \psi_\nu^{(\gamma)})}\int\int \mathbf{E}_\nu^{(\gamma)} \cdot \mathbf{E}_\mu^{*(\alpha)}\frac{\partial \varepsilon}{\partial z}dxdy. \tag{27}$$

If $\nu = \mu$, all the three terms contribute to the overall coupling coefficient $\vartheta_{\nu\nu}^{(\alpha,\gamma)}$. When α and γ are of different signs in the superscript, then this implies that a mode traveling in one direction will reflect part of its power. Equation (27) shows that the coupling coefficient is inversely proportional to the phase difference $(\phi_i^{(\tilde{a})} - \phi_i^{(\tilde{a})})$. For gradually varying geometrical variation waveguide, the phase difference varied very slowly and hence the coupling coefficient is very large indicating almost perfect transmission of lightwaves with negligible loss. On the other hand, an abruptly varying waveguide has a lower coupling coefficient due to the large phase difference. Another point to take note is that for real value of the phase coefficient, $\psi_\mu^{(\alpha)*}$, the modular in the numerator cancels out with the phase coefficient in the denominator. This means that the coupling between the guided modes is dependent on the phase difference. However, the coupling between radiation and guide modes does not cancel out. A fraction of power will also be loss to the radiation coupling.

In the next section, some issues that are concerned with the backward propagating waves will be discussed. This is because backward propagation waves are inevitable in all

geometrical variation structures. Therefore, it is important to understand the backward propagation waves for optimum coupling efficiency in tapered waveguide.

B. Backward propagating waves

In the whole derivation process, the backward traveling wave is not specifically discussed. It is natural to expect the presence of the backward traveling in any general solution of waveguide transmission. However, for the gradually varying waveguides, the backward propagating waves can be neglected. The coupling equation in Eq. (17) can be simplified as

$$\frac{\partial c_\mu^{(+)}}{\partial z}\exp(-i\psi_\mu z) - \frac{\partial c_\mu^{(-)}}{\partial z}\exp(i\psi_\mu z) = \sum_\nu R_{\nu\mu}[c_\nu^{(+)}\exp(-i\psi_\mu z) - c_\nu^{(-)}\exp(i\psi_\mu z)], \tag{28a}$$

$$\frac{\partial c_\mu^{(+)}}{\partial z}\exp(-i\psi_\mu z) - \frac{\partial c_\mu^{(-)}}{\partial z}\exp(i\psi_\mu z) = \sum_\nu S_{\nu\mu}[c_\nu^{(+)}\exp(-i\psi_\mu z) + c_\nu^{(-)}\exp(i\psi_\mu z)]. \tag{28b}$$

When Eq. (28) is applied to the taper waveguide with a gradual curvature, most of the coupling power is concentrated in the forward direction while the back reflected power (power flow in the backward direction) is very small. In this case, it is assumed that the reflected power can be neglected and then it has the amplitude coefficient $c_\mu^{(-)}=0$. However, this has caused some contradiction in Eq. (28) because now the derivative of $c_\mu^{(-)}$ is automatically zero. Substituting $c_\mu^{(-)}$ into Eq. (28), it is obtained as

$$R_{\nu\mu} = S_{\nu\mu}. \tag{28c}$$

The above equation is rather contradicting for the coupling coefficients, $R_{\nu\mu}$ and $S_{\nu\mu}$. If this is the case, then either of the equations in Eq. (28) appears to be redundant. The main reason why this issue is due to the assumptions made in the derivative of the backward traveling wave, $c_\mu^{(-)}$. The derivative of amplitude coefficient $c_\mu^{(-)}$ needs to be considered. Expressing the backward amplitude coefficient $c_\mu^{(-)}$ in terms of $c_\mu^{(+)}$, the coefficient of the backward amplitude can be expressed as

$$c_\mu^{(-)}(z) = -\int_{z_0}^{z_1} \frac{\partial c_\mu^{(+)}}{\partial z}\exp(-2i\psi_\mu z)dz. \tag{29}$$

The amplitude coefficient of backward traveling waves $c_\mu^{(-)}$ is dependent on the derivatives of the forward propagating amplitude coefficient, $\partial c_\mu^{(+)}/\partial z$. The backward waves cannot build up if the taper curvature has a gradual slope and $c_\mu^{(-)} \approx 0$. The exponential factor, $\exp(-2i\psi_\mu z)$, cancels the oscillation that arises from its own rapid oscillation. However, this does not give a good reason to neglect the derivative of $c_\mu^{(-)}$ even though it does not grow to appreciable values.

C. Radiation and guided mode coupling

In the previous section, the exact step-coupling theory is for coupling between the guided modes. However, there are other couplings between radiation and guided modes near the band edge. Hence, the coupling equations are modified. From Eq. (6), the series expansion of the electromagnetic field is re-expressed as

$$E_t = \sum_\nu p_\nu \mathbf{E}_{\nu t}\exp(-i\psi_\nu z) + \int_0^\infty p_\rho \mathbf{E}_{\rho t}\exp(-i\psi_\rho z)d\rho, \tag{30a}$$

$$H_t = \sum_\nu q_\nu \mathbf{H}_{\nu t}\exp(-i\psi_\nu z) + \int_0^\infty q_\rho \mathbf{H}_{\rho t}\exp(-i\psi_\rho z)d\rho. \tag{30b}$$

Equation (30) shows the full series expansion of the electromagnetic field including the radiation modes (integral form) and guided modes (summation form). Previously, the field expansion has real guided mode in the tapering section and the radiation mode expression is hidden. The radiation mode is only considered along the x direction when calculating the coupling efficiency at the band edge. The power transmitted through the "lossy" waveguide is given as

$$P_t = P\left[\sum_\nu (|c_\nu^{(+)}|^2 - |c_\nu^{(-)}|^2) - \sum\int_0^\infty (|c_\rho^{(+)}|^2 - |c_\rho^{(-)}|^2)d\rho\right]. \tag{31}$$

According to Eq. (31), the radiated power is subtracted from the transmission power. This is because lightwave power leaks into the crystal lattice when propagating through the lossy taper. At the reflection section (the section that contains a band gap), the coupling amplitude of backward propagating light is much larger than the forward amplitude, $c_\nu^{(-)} \gg c_\nu^{(+)}$. The integral extends over the whole propagating radiation modes. Since most light is reflected, it is expected that the radiation loss is always in the backward direction. Since the amplitudes $c_v^{(-)}$ and $c_\rho^{(-)}$ are larger than their positive counterparts, it is expected that the power P_t is negative. This implies that lightwaves are flowing backward.

D. PC structure with vertical mode confinement

The three-dimensional (3D) transmission of lightwaves in the PC slab is modeled by using the exact step-coupling theory. The coupling equations are quite similar to the two-dimensional (2D) PC structure. However there are two differences between the 3D and 2D models. First, the PC slab has a slightly different band diagram as compared to the 2D rods structure due to the presence of the lightcone. The presence of the lightcone in the dispersion band diagram has an additional insertion of continuum radiation states. All the modes that are above the lightcone are treated as bulk radiation modes, which are extended infinitely in the region above and below the slab. Therefore, the number of guided modes is reduced as some of these modes may exist in the region above the lightcone. The simulation time and computational

resources required for the PC slab are lesser. Second, the presence of two different guiding mechanisms in the 3D model for the PC slab implies that the field in Eqs. (3) and (4) needs to be redefined to account for the vertical confinement. However, the thickness of the slab is chosen to support one single mode for simplicity. The electromagnetic fields for the PC slab are redefined as

$$E_\nu = \left[\sum_\nu p_{\nu x}(\mathbf{E}_{\nu x})\exp\{-i[\psi_x(z)]z\}\right] + p_{\nu y}\mathbf{E}_y \exp\{-i[\beta_y(z)]z\}, \tag{32a}$$

$$H_\nu = \left[\sum_\nu q_{\nu x}(\mathbf{H}_{\nu x})\exp\{-i[\psi_x(z)]z\}\right] + q_{\nu y}\mathbf{H}_y \exp\{-i[\beta_y(z)]z\}. \tag{32b}$$

In Eq. (32), the separation of variables is used. The subscripts x and y refer to the electromagnetic fields in the transverse directions and z is the propagating direction. $\psi_x(z)$ is the propagation constant of the electromagnetic fields in the x direction that represents the guiding mechanism by defects modes in the photonic band gap. $\beta_y(z)$ is the propagation constant of the electromagnetic fields in the y direction that represents the index guiding mechanism in the PC slab. Equation (32) shows the simplified notation where all the guided and radiation modes in the PC slab are in the x direction while it only considers the radiation mode in air in the y direction. The new overall coupling coefficient is given by

$$\vartheta_{\nu\mu}^{(\alpha,\gamma)} = \frac{\omega\alpha|\psi_{\mu x}^{(\alpha)*} + \beta_y|}{2P(\psi_{\mu x}^{(\alpha)*} + \beta_y)(\psi_{\mu x}^{(\alpha)*} - \psi_{\nu x}^{(\gamma)})} \times \int\int \frac{\partial\varepsilon}{\partial z}[\mathbf{E}_{\nu x}^{(\gamma)}\mathbf{E}_{\mu x}^{(\alpha)*} + |\mathbf{E}_y|^2]dxdy. \tag{32c}$$

The overall coupling coefficient Eq. (32c) does not really differ much from the original equation shown in Eq. (27) except the electromagnetic fields are divided into the x and y directions. Due to the lack of symmetry in the vertical direction, the modes cannot be purely TM or TE polarized. Therefore, the guided modes are still classified into even or odd modes, with respect to the reflections through the horizontal plane of the PC slab.

III. NUMERICAL SIMULATION RESULTS AND DISCUSSIONS

In this section, numerical case study using the exact step-coupling equation is verified. The simulation results of the exact step-coupling equation are compared with the simulation results from the modified step-theory and the scattering method for identical PC structure. The percentage error of the modified step theory and the exact step-coupling equation are obtained with reference to the scattering method. Subsequently, the exact step-coupling equations are applied to other PC slab taper and lossy structures to simulate and calculate the transmission efficiency.

A. Applying the exact step-coupling model to the numerical examples

The ψ_ν values are obtained from the respective band structures, which are calculated from each step width using the plane-wave method.[31] There is a large number of ψ values for all the modes and frequencies in each step width. This is reduced by considering only the even field mode distribution because the tapered waveguide is symmetric about the x axis. The lowest order fundamental mode and intermediate higher order modes (up to the fifth order even mode) are considered in this paper. Such simplification reduces the simulation time and is effective for symmetrical and long PC tapered waveguide.[21] The transmission efficiency is calculated iteratively using Eq. (27) from the first step width at the front to the last step at the transmission collection location for the whole tapered waveguide section. The final field amplitude at the end of the narrow PCTW is normalized with incident power to obtain the transmission efficiency at different frequencies. In the simulation, the step width is defined as one column of cell structures as shown in Fig. 3(a).

B. Convergence of linear defect twin input/output PCTW

In this section, the exact step-coupling theory is verified for convergence. The PC structure is the linear PCTW with a row of defects in the tapering section shown in Fig. 3(a).[21] The structure is called a twin input/output PCTW because the waveguide decreases in width and then opens up in the opposite side. The parameters of the twin input/output PCTW are given in Ref. 21. Based on the case study as shown in Fig. 3(a), the input and output twin PCTWs are modeled using the exact step-coupling theory and compared with the modified step-theory and scattering matrix method[20,40,41] for verification in Fig. 3(b). The numerical simulation results of the transmission spectrum are obtained at the end of the input tapered waveguide as shown in Fig. 3(a). There is some deviation between the modified step theory (in dash-dotted line) and the scattering method. This is particularly true nearer the band edge. The simulation results of the exact step-coupling theory (in circular symbol) are in very good agreement with the scattering method. With reference to the scattering method,[20] the numerical error for the modified step theory is approximately 3.44%. This is higher than the percentage error of the exact step-coupling theory, especially nearer to the band edge as shown in Fig. 3(c). The exact step-coupling theory shows very high accuracy with a percentage error less than $\pm 0.28\%$. This is because the exact step-coupling theory is derived directly from the Maxwell equations but the modified step theory is from scalar waveguide solution. It also shows that the small set of modes is enough to form a complete set for the expansion of the tapered modes with small errors. It also shows that the exact step-coupling theory converges and is more accurate than the modified step theory. It also demonstrates that by considering unperturbed taper mode up to only the fifth order, it would be sufficient enough to obtain reasonably high accuracy.

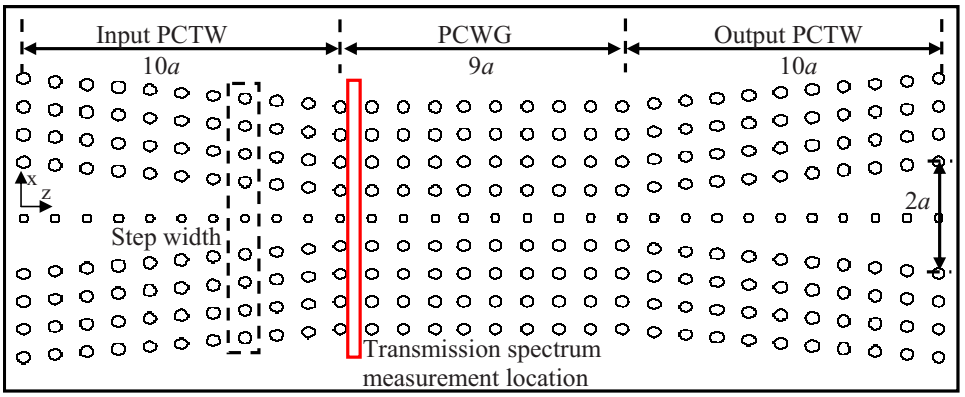

(a)

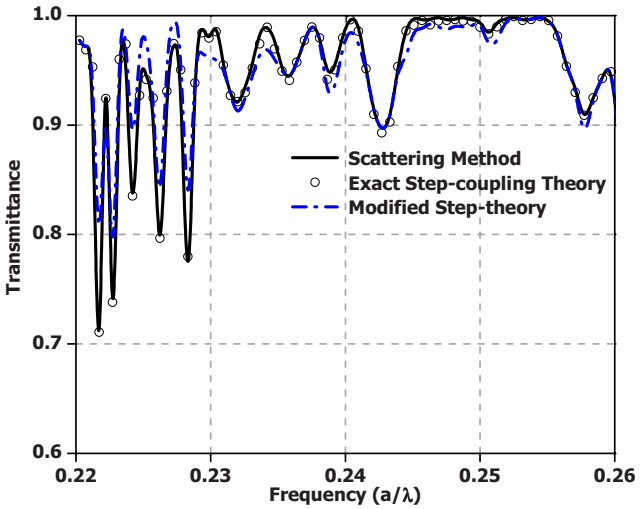

(b)

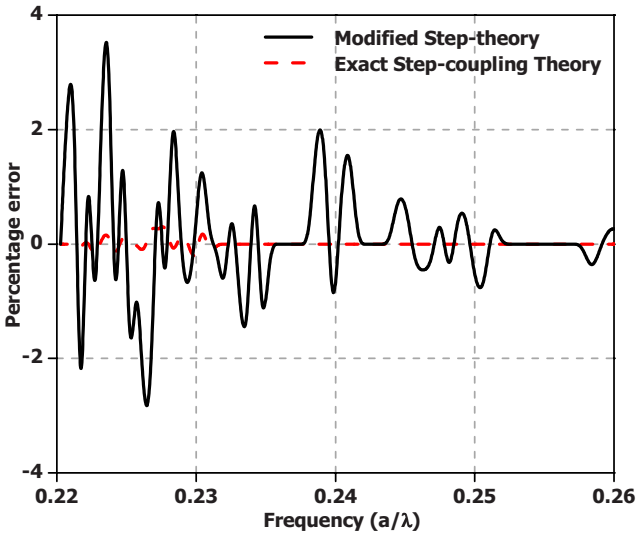

(c)

FIG. 3. (Color online) (a) Structure of the twin input/output linear defect PCTW. (b) Transmission spectrum of the twin input/output linear defect PCTW. (c) Percentage error for the transmission spectrum.

C. Lossy photonic crystal waveguide

In this section, the exact step-coupling theory is used to calculate the transmission spectrum of nonadiabatic and lossy PCTW (Ref. 20) as shown in Fig. 4(a). The radius of the rods in the cladding of the PCTW is gradually increased to form a transition structure as "turning on" the crystal. Hereafter, this structure is called "turn-on" PCTW. The unperturbed rods have a r/a ratio of 0.3 with a refractive index of 3.37. The line defects rods have a r/a ratio of 0.2. The transmission coupling efficiency of the turn-on PCTW is ob-

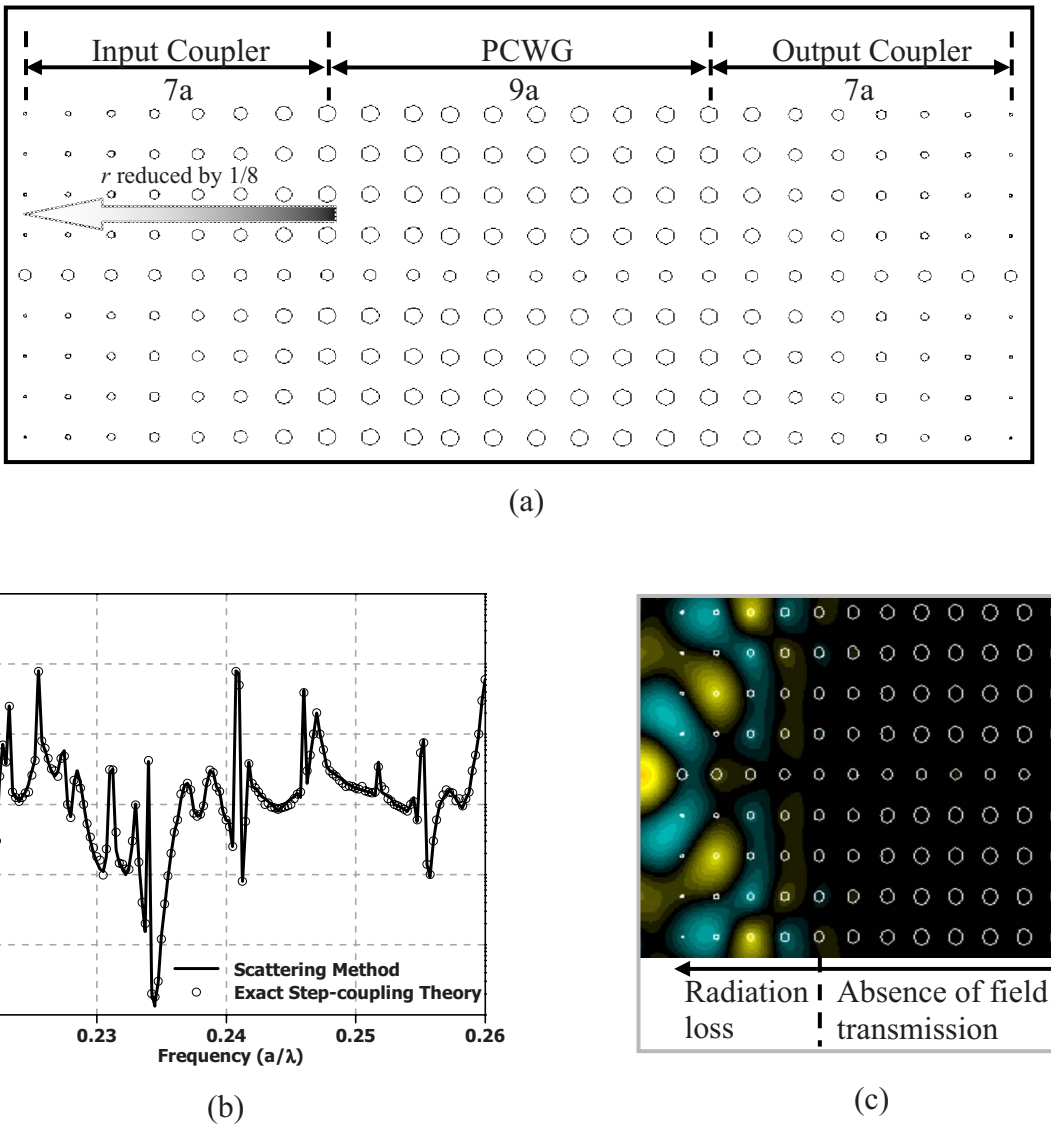

FIG. 4. (Color online) (a) Schematic of the turn-on PCTW structure. (b) Transmission spectrum of the turn-on PCTW structure. (c) Field plot of the design showing coupling of the back reflected light to the radiation modes in the cladding.

tained from the middle of the structure using the step-coupling theory. This PCTW structure has a very low coupling efficiency in the transmission spectrum as shown in Fig. 4(b). The low transmission coupling efficiency is due to the absence of the guided modes in one section of the turn-on PCTW. In order to design an effective PCTW to provide high coupling efficiency, at least one guided mode must be present in every intermediate section of the tapering structure. In this turn-on PCTW structure, one section does not have at least one guided mode of the condition. This is due to the geometrical coincident of the line defect radius with the radius of the cladding rods. Lightwaves are reflected in this part of the turn-on section. From the physical point of view, due to the turning effect of the cladding, the radiation modes from the edge of bulk continuum of states above the photonic band gap are pulled down by the increasing rod size. This radiation mode continues to sink deeper into the band gap along the turn-on section and then eventually crosses the operating mode in the linear defects. Therefore, the original mode is unguided and thus light is reflected and radiated out resulting in low transmission over the whole spectrum.

The exact step-coupling theory can be applied to analyze the low power transmission in Fig. 4(b). In this case, the radiation modes play an important role and are treated carefully to avoid any miscalculation. Figure 4(c) shows the distribution of the back reflected field radiating out in the backward direction from the reflection section. It shows the coupling between the reflected field and the radiation field in the turn-on section. It is clearly shown that the radiated electromagnetic field is present in the cladding of the turn-on PCTW. Therefore, the reflected field is coupled into the bulk radiated field in the PC structure above and below the row defect as radiation loss.

D. Photonic crystal slab taper

Previously, all the simulation results are based on a 2D PCTW with rods structure. For practical applications, peri-

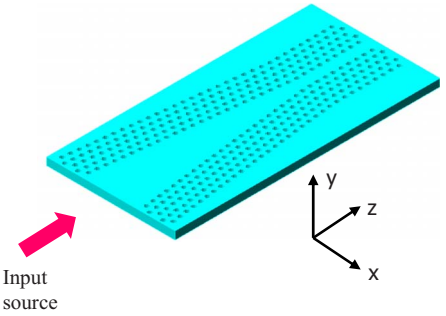

FIG. 5. (Color online) 3D diagram of the PC slab tapered waveguide.

odic 3D PC structures are often considered due to the existent of a three-dimensional photonic band gap. However, the fabrication of 3D periodic PC structures is a challenge because of the complexity of its process and strict alignment requirements.[42–44] As such, a semi-three-dimensional PC slab[5,45] is proposed.

In this paper, the photonic crystal slab consists of silicon material with refractive index 3.5. The slab thickness is 0.3 μm approximately, which ensures that the transverse field remains single mode while being strongly guided in the vertical direction.[5,45] The lattice structures are made up of air holes arranged in a triangular pattern. The radius to lattice constant ratio is set to $r/a=0.3$. As a result, the photonic band gap is in the range of normalized frequencies of 0.22–0.275 for the TE polarization.

The PCTW structure is created using the shearing method as that in the square rods lattice structure.[31] However, due to the difference in the lattice arrangement (which is square for rods and triangular for holes), the holes are shifted in a different manner. In the square case, the horizontal and vertical lattice vectors are perpendicular to each other. For the triangular pattern, the angle between the vectors is at 60°. Hence the shifting must maintain the lattice angle of 60°. Figure 5 shows the case of 3D linear photonic crystal slab taper (PCST). The input width of PCST is approximately 3 μm, which corresponds to the mode size of a tapered fiber. The output width is a PCWG with one missing row of hole structures (W1). Figures 6(a) and 6(b) show the mode distribution in the vertical direction and the percentage of the power coupled into the width of 0.3 μm thickness slab for a 3 μm input mode size. It can be only approximately 20% of the total power that is fed into the thin slab waveguide. The remaining power is reflected backward to the source or radiate out in the air above and below the slab.

Figure 7(a) shows the different curvatures of the tapered waveguide such as linear, convex, and concave.[21,31] Simulations are performed to obtain the transmission spectra of the linear, convex, and concave tapers for a taper length of 18a as shown in Fig. 7(b). The transmission spectrum is calculated for the case where α and γ are positive (in the forward direction). The coupling coefficient in Eq. (32c) is used to calculate the transmission spectrum at the normalized frequency range of 0.24–0.27. The transmission coupling efficiency is normalized with respect to the amount of power coupled into the slab. As seen from Fig. 7, the convex taper gives the highest overall coupling efficiency due to its

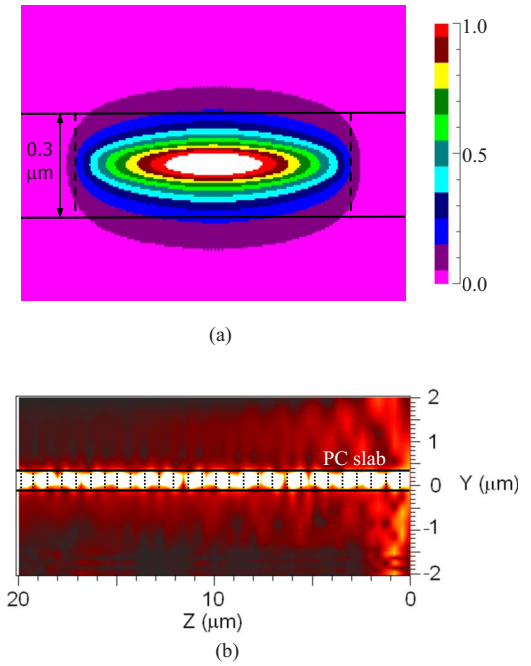

FIG. 6. (Color online) Vertical mode profile of the electromagnetic field in the PC slab (a) back view. (b) Side view.

gradual curvature, while the concave taper gives the lowest due to its very fast tapering rate in the front part. The linear PCST has results in between the convex and concave taper. This is because the linear PCST has moderate curvature. As a result, the loss and transmission power are not as extreme as the concave and convex tapers. As mentioned in Refs. 21 and 31 the fluctuations in the spectrum are due to the presence of multiple reflections from Fabry-Perot oscillation or multipath interference. The concave taper has more fluctuations due to the inward curvature. This results in much higher reflections and interferences in the concave taper, hence more fluctuations. For the convex taper, it is the opposite and therefore exhibits more stable spectrum. As the taper length increases, the fluctuations will be gradually reduced and a stable transmission spectrum can be obtained. This is desirable because a stable transmission spectrum allows more reliable and better performance.

To further study the influence of the taper length, Fig. 8 shows the transmission efficiency of the three taper curvatures as a function of the taper lengths at the normalized frequency of $0.258(a/\lambda)$. The maximum taper length is capped at 28a. This is because longer tapers defeat the purpose of a compact input/output port for PC devices as well as introducing additional radiation loss around the slab. The beam reduction ratio for the PC slab taper is smaller, hence shorter taper length is required to obtain high coupling efficiency. From Fig. 8, it is observed that generally there are oscillations at shorter taper lengths. This is due to the presence of a large number of interferences and reflections at the shorter taper length. The convex taper achieves 90% coupling efficiency at a taper length of 20a while the linear reaches 90% at 26a. The coupling efficiency of the concave taper reaches 87% at 28a. It is worth noting that although the convex taper produces higher coupling efficiencies for both

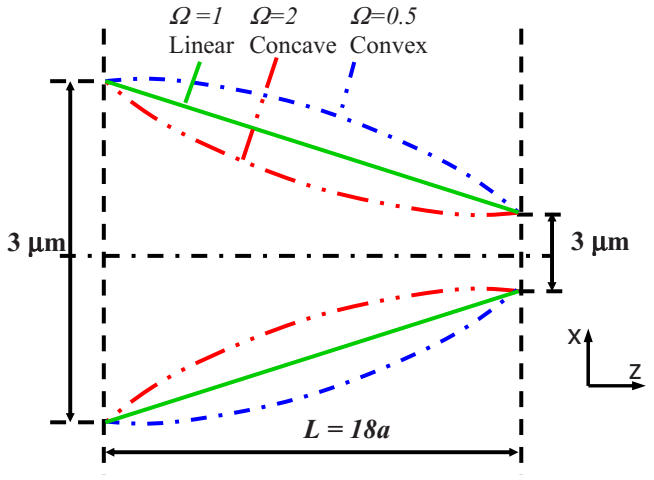

(a)

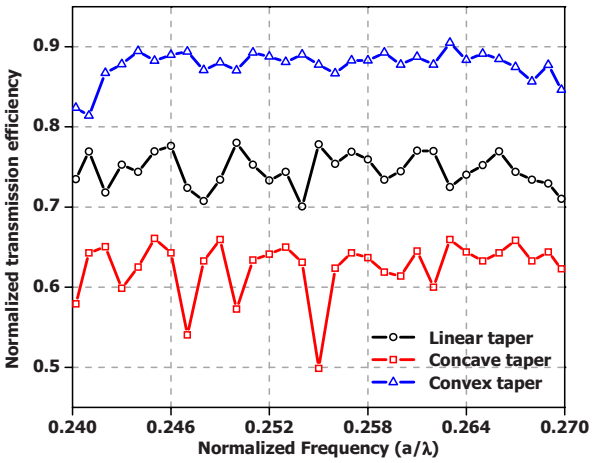

(b)

FIG. 7. (Color online) (a) Schematic layout of the linear, convex, and concave tapers. (b) Transmission spectra of the PC slab tapered waveguide for the linear, concave, and convex tapers at a length of 18*a*.

the 2D PCTW and 3D PCST, the actual power transmission is different and that of the PCST is slightly lower.

IV. CONCLUSIONS

In this paper, an exact step-coupling theory is developed for calculating the transmission efficiency in geometrical variation PCWGs. This theory captures the essentials of the classical coupled mode theory and the step theory and arrives at a set of generalized coupling equations, which give a complete description of the field modal behavior for the propagation of lightwaves in geometrical variation PCWGs. The effectiveness of the exact step-coupling theory is verified by the specially chosen case studies. It demonstrates quick and accurate convergence in dealing with the twin input/output PCTW and linear curvature PCTW. It also matches well with the scattering method in calculating the lossy turn-on PCTW structures. When it is applied to the 3D PCSTs, this theory shows good capability in predicting the transmission spectra and the efficiencies of the linear, convex, and concave PCSTs. Compared with the available methods, the exact step-coupling theory is applicable to a vast range of geometrical variation PCWGs, quick and accurate convergence simulation results, as well as complete solution for the intermodal coupling mechanism.

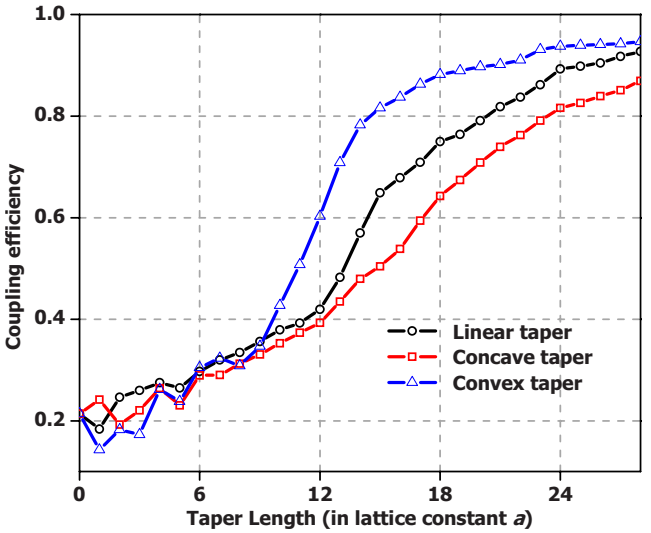

FIG. 8. (Color online) Transmission efficiency vs taper length of the PC slab tapered waveguide for the linear, concave, and convex tapers.

ACKNOWLEDGMENTS

The authors express their sincerest gratitude to Steven G. Johnson from MIT for his friendly advice and useful discussion.

*Corresponding author. FAX: (65) 6793-3318; eaqliu@ntu.edu.sg

[1] J. N. Winn, Y. Fink, S. Fan, and J. D. Joannopoulos, Opt. Lett. **23**, 1573 (1998).
[2] P. R. Villeneuve, S. Fan, S. G. Johnson, and J. D. Joannopoulos, IEE Proc., Optoelectron. **145**, 384 (1998).
[3] M. Soljačić, S. G. Johnson, S. Fan, M. Ibanescu, E. Ippen, and J. D. Joannopoulos, J. Opt. Soc. Am. B **19**, 2052 (2002).
[4] H. Benisty, J. Appl. Phys. **79**, 7483 (1996).
[5] S. G. Johnson, P. R. Villeneuve, S. H. Fan, and J. D. Joannopoulos, Phys. Rev. B **62**, 8212 (2000).
[6] A. Mekis, J. C. Chen, I. Kurland, S. Fan, P. R. Villeneuve, and J. D. Joannopoulos, Phys. Rev. Lett. **77**, 3787 (1996).
[7] S. Fan, P. R. Villeneuve, J. D. Joannopoulos, and H. A. Huas, Opt. Express **3**, 4 (1998).

[8] M. Bayindir, B. Temelkuran, and E. Ozbar, Appl. Phys. Lett. **77**, 3902 (2000).
[9] Y. Akahane, M. Mochizuki, T. Asano, Y. Tanaka, and S. Noda, Appl. Phys. Lett. **82**, 1341 (2003).
[10] M. Soljacic, M. Ibanescu, S. G. Johnson, Y. Fink, and J. D. Joannopoulos, Phys. Rev. E **66**, 055601(R) (2002).
[11] D. Taillaert, W. Bogaerts, P. Bienstman, T. Krauss, P. V. Daele, I. Moerman, S. Verstuyft, K. D. Mesel, and R. Baets, IEEE J. Quantum Electron. **38**, 949 (2002).
[12] P. E. Barclay, K. Srinivasan, M. Borselli, and O. Painter, Opt. Lett. **29**, 697 (2004).
[13] D. W. Prather, J. Murakowski, S. Shi, S. Venkataraman, C. Chen, and D. Pustai, Opt. Lett. **27**, 1601 (2002).
[14] O. Mitomi, K. Kasaya, and H. Miyazawa, IEEE J. Quantum Electron. **30**, 1787 (1994).
[15] B. Luyssaert, P. Bienstman, P. Vandersteegen, P. Dumon, and R. Baets, J. Lightwave Technol. **23**, 2462 (2005).
[16] A. Mekis and J. D. Joannopoulos, J. Lightwave Technol. **19**, 861 (2001).
[17] Y. Xu, R. K. Lee, and A. Yariv, Opt. Lett. **25**, 755 (2000).
[18] T. D. Happ, M. Kamp, and A. Forchel, Opt. Lett. **26**, 1102 (2001).
[19] P. Pottier, I. Ntakis, and R. M. De La Rue, Opt. Commun. **223**, 339 (2003).
[20] S. G. Johnson, P. Bienstman, M. A. Skorobogatiy, M. Ibanescu, E. Lidorikis, and J. D. Joannopoulos, Phys. Rev. E **66**, 066608 (2002).
[21] E. H. Khoo, A. Q. Liu, and J. H. Wu, Opt. Express **13**, 7748 (2005).
[22] Ph. Lalanne and A. Talneau, Opt. Express **10**, 354 (2002).
[23] M. Palamaru and Ph. Lalanne, Appl. Phys. Lett. **78**, 1466 (2001).
[24] R. J. P. Engelen, Y. Sugimoto, Y. Watanabe, J. P. Korterik, N. Ikeda, N. F. van Hulst, K. Asakawa, and L. Kuipers, Opt. Express **14**, 1658 (2006).
[25] S. G. Johnson, M. Ibanescu, M. Skorobogatiy, O. Weisberg, J. D. Joannopoulos, and Y. Fink, Phys. Rev. E **65**, 066611 (2002).
[26] M. Skorobogatiy, M. Ibanescu, S. G. Johnson, O. Weisberg, T. D. Engeness, M. Soljačić, S. A. Jacobs, and Y. Fink, J. Opt. Soc. Am. B **19**, 2867 (2002).
[27] M. Koshiba, Y. Tsuji, and M. Hikari, J. Lightwave Technol. **18**, 102 (2000).
[28] G.-W. Chern, L. A. Wang, and C.-Y. Lin, Appl. Opt. **40**, 4476 (2001).
[29] Z. Y. Li and K. M. Ho, Phys. Rev. B **68**, 155101 (2003).
[30] A. R. Nelson, Appl. Opt. **14**, 3012 (1975).
[31] E. H. Khoo, A. Q. Liu, J. H. Wu, J. Li, and D. Pinjala, Opt. Express **14**, 6035 (2006).
[32] K. Sakoda, *Optical Properties of Photonic Crystal* (Springer-Verlag, Berlin, 2001).
[33] B. Z. Katsenelenmbaum, L. Mercader del Río, M. Pereyaslavets, M. Sorolla Ayza, and M. Thumm, *Theory of Nonuniform Waveguides: The Cross-Section Method* (Institute of Electrical Engineers, London, 1998).
[34] J. David Jackson, *Classical Electrodynamics* (John Wiley & Sons, New York, 1998).
[35] D. Marcuse, *Theory of Dielectric Optical Waveguide* (Academic Press, San Diego, 1991).
[36] S. Wilcox, L. C. Botten, R. C. McPhedran, C. G. Poulton, and C. M. de Sterke, Phys. Rev. E **71**, 056606 (2005).
[37] G. Reiter, Proc. Inst. Electr. Eng. **106B**, 54 (1959).
[38] F. Sporleder and H. G. Unger, *Waveguide Tapers, Transitions, and Couplers* (Peter Peregrinus, New York, 1974).
[39] D. Marcuse, Bell Syst. Tech. J. **49**, 273 (1969).
[40] G. Tayeb and D. Maystre, J. Opt. Soc. Am. A Opt. Image Sci. Vis **14**, 3323 (1997).
[41] J. Yonekura, M. Ikeda, and T. Baba, J. Lightwave Technol. **17**, 1500 (1999).
[42] E. Yablonovitch, T. J. Gmitter, and K. M. Leung, Phys. Rev. Lett. **67**, 2295 (1991).
[43] S. Fan, P. R. Villeneuve, R. Meade, and J. D. Joannopoulos, Appl. Phys. Lett. **65**, 1466 (1994).
[44] H. S. Sözüer and J. P. Dowling, J. Mod. Opt. **41**, 231 (1994).
[45] S. G. Johnson, S. Fan, P. R. Villeneuve, J. D. Joannopoulos, and L. A. Kolodziejski, Phys. Rev. B **60**, 5751 (1999).